Chinese Chemical Letters 37 (2026) 111230

Contents lists available at ScienceDirect

Chinese Chemical Letters

journal homepage: www.elsevier.com/locate/cclet

Cobalt-kernelled icosahedral gold nanocluster

Hao Liu[a,1], Kang Li[b,1], Fengyi Li[a,1], Yan Zhao[a], Weigang Fan[a], Yong Pei[b,*], Man-Bo Li[a,*]

[a] Institutes of Physical Science and Information Technology, Key Laboratory of Structure and Functional Regulation of Hybrid Materials of Ministry of Education, Anhui University, Hefei 230601, China
[b] Department of Chemistry, Key Laboratory of Environmentally Friendly Chemistry and Applications of Ministry of Education, Xiangtan University, Xiangtan 411105, China

ARTICLE INFO

Article history:
Received 4 March 2025
Revised 10 April 2025
Accepted 16 April 2025
Available online 17 April 2025

Keywords:
Nanocluster synthesis
Nanocluster catalysis
Cobalt
Metal doping

ABSTRACT

We report herein the synthesis, structure and catalysis of a cobalt-kernelled icosahedral gold nanocluster $CoAu_{12}$, providing an opportunity for the in-depth understanding of rarely reported Co-doped gold nanoclusters. $CoAu_{12}$ possesses a symmetric and contracted metal kernel compared to the 4d and 5d metal-kernelled MAu_{12} nanoclusters (M = Pd, Pt, Rh, Ir, Au), thus exhibiting highly structural stability. Meanwhile, $CoAu_{12}$ demonstrates efficient energy and electron transfer activity toward oxygen, thus endowing this nanocluster with exceptional catalytic activity in converting oxygen to singlet oxygen as well as superoxide. Structural features such as the unpaired electron of $CoAu_{12}$ have been verified as contributing to its catalytic activity. Efficient organic transformations involving singlet oxygen and superoxide were developed based on the structurally stable and catalytically active $CoAu_{12}$ nanocluster.

© 2026 Published by Elsevier B.V. on behalf of Chinese Chemical Society and Institute of Materia Medica, Chinese Academy of Medical Sciences.

The icosahedral Au_{13} composed of thirteen gold atoms has been revealed as a basic structure unit in atomically precise gold nanoclusters. Typical examples include $Au_{25}(SR)_{18}$, $Au_{25}(PPh_3)_{10}Br_5$, $Au_{42}(SR)_{32}$, *etc.* [1–6]. The investigation based on the Au_{13} unit triggers the discovery of various metal nanoclusters with intriguing properties [7–21]. On the other hand, the icosahedral Au_{13} is a stable form of nanoclusters as well [22–25]. This kind of nanoclusters such as $Au_{13}(NHC)_8Br_4$ (NHC = *N*-heterocyclic carbene) and $Au_{13}(SbPh_3)_8Cl_4$ have also been extensively studied. Apart from the monometallic gold nanoclusters, their doping analogues constitute a versatile platform for precisely modulating properties of the Au_{13} system at atomic level. In this context, metals that possess the similar atomic radii to Au have been successfully doped into the Au_{13} system by the methods of *in-situ* synthesis, anti-galvanic reduction (AGR), *etc.* [26–33]. The as-obtained metal nanoclusters such as $Au_{24}Cd(SR)_{18}$, $Au_{24}Hg(SR)_{18}$ and $Au_{36}Pd_2(SR)_{24}$ demonstrate significantly different properties compared to their gold analogues. In spite of the progress, the successful doping of cobalt into the Au_{13} system is rarely reported. One of the reasons might be that the cobalt is slightly far away from Au on the periodic table and possesses significantly different atomic radii and properties. Thus, the structural features and property characteristics of Co-doped gold nanoclusters are quite unknown.

Our group focuses on the construction of functional metal nanoclusters with bidentate phosphine ligands. By modifying the chain length and substituents of the bidentate phosphines, we realized the construction of gold and doped nanoclusters with diversified compositions [34–40]. Their atomically precise structures were revealed and practical applications in kinetic resolution, catalysis, chiral recognition, *etc.*, were developed as well. Recently, Tsukuda *et al.* synthesized a series of 4d and 5d metals doped MAu_{12} nanoclusters (M = Pd, Pt, Rh, Ir) and systematically investigated and compared their electronic structures, photoluminescence and catalytic performance [41–44]. Inspired by their elegant work, we are very interested in investigating the Co-doped icosahedral gold nanoclusters. Herein, we report this kind of nanocluster and reveal its structural features, electronic properties and photocatalytic activity.

Our attempt for the synthesis of cobalt-doped gold nanoclusters was initiated by following the procedure [43] described by Tsukuda *et al.* and replacing the 4d or 5d metal precursors by a cobalt precursor. Specifically, 1,2-bis(diphenylphosphino)ethane (dppe) and $Co(NO_3)_2$ were used as the ligand and cobalt precursor, respectively. However, a $[Au_{13}(dppe)_5Cl_2]^{3+}$ nanocluster [45] was always obtained as the final product no matter how the reaction conditions such as the temperature, solvent and reductant were changed (Fig. S1 in Supporting information). Considering that the atomic radius of cobalt is dramatically smaller than

* Corresponding authors.
E-mail addresses: ypnku78@gmail.com (Y. Pei), mbli@ahu.edu.cn (M.-B. Li).
[1] These authors contributed equally to this work.

https://doi.org/10.1016/j.cclet.2025.111230
1001-8417/© 2026 Published by Elsevier B.V. on behalf of Chinese Chemical Society and Institute of Materia Medica, Chinese Academy of Medical Sciences.

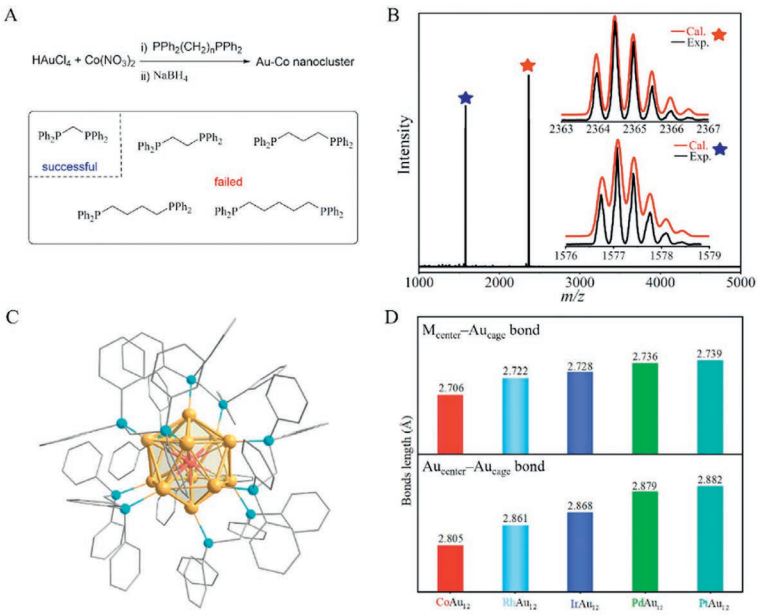


Fig. 1. (A) Synthetic procedure of $CoAu_{12}$ nanocluster. (B) ESI-MS spectrum of $CoAu_{12}$ nanocluster. (C) Total structure of $CoAu_{12}$ nanocluster. Color label: Au = yellow; Co = red; P = cyan; C = gray. H atoms are omitted for clarity. (D) Bonding information comparison of MAu_{12} nanoclusters (M = Co, Rh, Ir, Pd, Pt).

that of 4d and 5d metals, we envisioned that the cobalt-doped gold nanocluster would possess a smaller size and shorter metal–metal distances. Based on this analysis, we tried replacing dppe with bis(diphenylphosphino)methane (dppm), which has a shorter phosphine–phosphine distance and would match with the metal–metal distances of the Co-doped gold nanocluster. Delightedly, this strategy worked, and the replacement of dppe by dppm successfully led to the formation of a Co-doped nanocluster instead of Au_{13}. Similar bidentate phosphines with longer phosphine–phosphine bonds failed to give the desired nanocluster (Fig. 1A, Table S1 and Fig. S2 in Supporting information).

With optimized reaction conditions, the Co-doped nanocluster was synthesized and purified efficiently (details in Supporting information), enabling its 100 mg-scale preparation and further structural and property investigations. The molecular formula of the nanocluster was determined by electrospray ionization mass spectrometry (ESI-MS) to be $CoAu_{12}(dppm)_6$ (abbreviated as $CoAu_{12}$). Notably, two dominant peaks on positive mode were observed, which are assigned to $[CoAu_{12}(dppm)_6]^{3+}$ and $[CoAu_{12}(dppm)_6]^{2+}$, respectively (Fig. 1B). Different ESI-MS testing methods were tried and the two peaks always appeared simultaneously (Fig. S3 in Supporting information). Single crystal X-ray diffraction (SCXRD) revealed the atomically precise structure of $CoAu_{12}$ and further confirmed its composition. This nanocluster crystallizes in the trigonal space group *P*-31*c* (crystal data, see Table S2 in Supporting information), possessing a symmetrically icosahedral geometry (Fig. 1C and Fig. S4 in Supporting information). A Co atom is located at the center of the icosahedron, while twelve Au atoms surround the cobalt atom and constitute the twelve vertices of the icosahedron. The average distance from the central Co atom to the twelve Au atoms (M_{center}-Au_{cage}) is 2.706 Å (Fig. 1D). Meanwhile, the average Au-Au distance on the surface of the icosahedron (Au_{cage}-Au_{cage}) is determined to be 2.805 Å. Based on the bond length analysis (Fig. 1D), $CoAu_{12}$ is more symmetric than 4d and 5d metal-doped MAu_{12} nanoclusters (M = Rh, Ir, Pd, Pt, Au) [45,46]. We compared the average M_{center}-Au_{cage} (M = doped metal) and Au_{cage}-Au_{cage} distances of $CoAu_{12}$, $RhAu_{12}$, $IrAu_{12}$, $PdAu_{12}$ and $PtAu_{12}$. The results indicate that apart from the highest symmetry, $CoAu_{12}$ possesses the most contracted

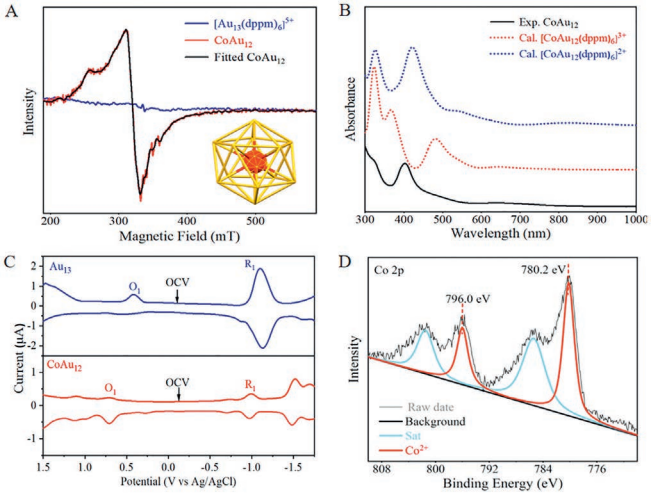


Fig. 2. (A) EPR spectrum of $CoAu_{12}$ and Au_{13} nanoclusters (Inset: the calculated spin density distribution of $CoAu_{12}$ showing that the red isosurface is mainly distributed at the center of $CoAu_{12}$). (B) Experimental and simulated UV−vis spectra of $CoAu_{12}$ nanocluster. (C) DPV spectra of $CoAu_{12}$ and Au_{13}. (D) Co2p XPS spectrum of $CoAu_{12}$ nanocluster.

structure among the reported MAu_{12} nanoclusters (Fig. S5 in Supporting information). This observation further confirms our envision in the synthesis of $CoAu_{12}$ that this nanocluster would possess a smaller size and shorter metal–metal distances, and also explains the interesting phenomenon that only dppm with a shorter phosphine–phosphine distance is feasible for the construction of $CoAu_{12}$ nanocluster.

Concerning the valence state of $CoAu_{12}$, two observed counter ions in the crystal data suggest that this nanocluster is +2 (Fig. S4A). The electron paramagnetic resonance (EPR) result confirms this conclusion, because obvious magnetic signal was observed for $CoAu_{12}$ (Fig. 2A). Based on the electronic configuration of Au ($[Xe]4f^{14}5d^{10}6s^1$) and Co ($[Ar]3d^74s^2$), $CoAu_{12}$ shows EPR signal only when it is even-valence charged. Therefore, the

$[CoAu_{12}(dppm)_6]^{3+}$ peak observed in ESI-MS is probably due to ionization under ESI conditions, rather than being the native charge. For comparison, we prepared a structurally similar and monometallic $[Au_{13}(dppm)_6]^{5+}$ nanocluster (abbreviated as Au_{13}) based on the previous report (for its synthesis, see Supporting information) [47,48]. This nanocluster possesses a closed-shell electronic structure (13e – 5e = 8e), and showed no signal in the EPR spectrum (Fig. 2A). Apart from the experimental results, density functional theory (DFT) calculations indicate that the simulated absorption spectrum of $[CoAu_{12}(dppm)_6]^{2+}$ matches well with the experimental one (Fig. 2B), while $[CoAu_{12}(dppm)_6]^{3+}$ showed distinct absorption peaks. The theoretical results further suggest the +2 valence of the obtained $CoAu_{12}$ nanocluster. Notably, we also simulated the UV–vis spectrum of the triplet state of $[CoAu_{12}(dppm)_6]^{3+}$ (Fig. S13 in Supporting information). The distinct simulated absorption peaks from the experimental data also rule out the possibility of +3 valence state of $CoAu_{12}$ nanocluster. Based on the above evidence, this is the first time we discover a stable icosahedral M_{13} nanocluster that disobeys the octet rule (8e valence electrons) [49,50].

Notably, the cobalt atom in $CoAu_{12}$ does not contribute electrons, Instead, it accepts one electron to form full-filled d orbitals. Thus, the free electrons of $[CoAu_{12}]^{2+}$ should be 12 – 1 – 2 = 9. The origin of stability of $[CoAu_{12}(dppm)_6]^{2+}$ (9e) can be explained by three aspects. First, we conducted the differential pulsed voltammetry (DPV) of $CoAu_{12}$. The DPV spectrum of Au_{13} was also obtained for comparison. From the spectra (Fig. 2C), the first oxidation potential (O_1) of $CoAu_{12}$ (0.72 V *vs.* Ag/AgCl) is more positive than that of Au_{13} (0.48 V *vs.* Ag/AgCl), indicating that $CoAu_{12}$ is more difficult to be oxidized. Meanwhile, the first reduction potential (R_1) of $CoAu_{12}$ (−0.97 V *vs.* Ag/AgCl) is also more positive than that of Au_{13} (−1.13 V *vs.* Ag/AgCl), demonstrating that $CoAu_{12}$ is more easily to be reduced. The redox properties suggest that $CoAu_{12}$ favors a lower +2 valence state instead of $[CoAu_{12}(dppm)_6]^{3+}$. Second, based on the X-ray photoelectron spectroscopy (XPS) result of $CoAu_{12}$, the deconvoluted Co 2p XPS spectrum showed intensive Co signals at 796.0 and 780.2 eV (Fig. 2D). The binding energy and satellite peaks (Sat) all suggest a Co^{2+} in the $CoAu_{12}$ nanocluster. The calculated spin density distribution (Fig. S14 in Supporting information) of $CoAu_{12}$ also shows that the red isosurface is mainly distributed at the center of $CoAu_{12}$, *i.e.*, Co atom (Fig. 3A, inset). In other words, the unpaired electron of $CoAu_{12}$ comes from the doped Co atom. Therefore, $CoAu_{12}$ favors holding one excess electron under normal conditions as the relatively stable Co^{2+} compared to Co^{3+}. Third, based on the SCXRD analysis, $[CoAu_{12}(dppm)_6]^{2+}$ possesses a contracted and symmetric structure. The calculated bond orders of Au_{cage}-Au_{cage} bonds on the Au_{12} cage of $CoAu_{12}$ is generally larger than that of Au_{13} (Fig. S15a in Supporting information), probably due to the smaller radius of the Co atom resulting in a more compact core. The strong Au-Au interactions on the surface also lead to the high stability of $[CoAu_{12}(dppm)_6]^{2+}$. Interestingly, the bond orders of Co_{center}-Au_{cage} bonds in $CoAu_{12}$ are smaller than that of Au_{center}-Au_{cage} bonds in Au_{13} (Fig. S15b in Supporting information), suggesting the relatively weaker Co-Au interactions.

The stability of $CoAu_{12}$ nanocluster under different conditions was then verified by UV–vis spectra. It was shown that the absorption curves of $CoAu_{12}$ dissolved in dichloromethane kept unchanged even for seven days. Especially, UV–vis results indicate that $CoAu_{12}$ possesses highly structural stability toward atmospheric oxygen and light irradiation (Figs. S6 and S7 in Supporting information). The high stability of $CoAu_{12}$ under oxidation and irradiation conditions inspires us to further explore the catalytic performance of $CoAu_{12}$ in photo-induced oxidation reactions. Previous results have shown that Au_{13} unit-based nanoclusters have the potential to activate the oxygen molecule under irradiation, generating singlet oxygen that is able to efficiently oxidize the tetrahydroisoquinoline and sulfides [51]. However, stability issue results in their decomposition under light irradiation. The high stability of $CoAu_{12}$ toward both oxidation and light irradiation conditions is beneficial for its application in photo-induced oxidations.

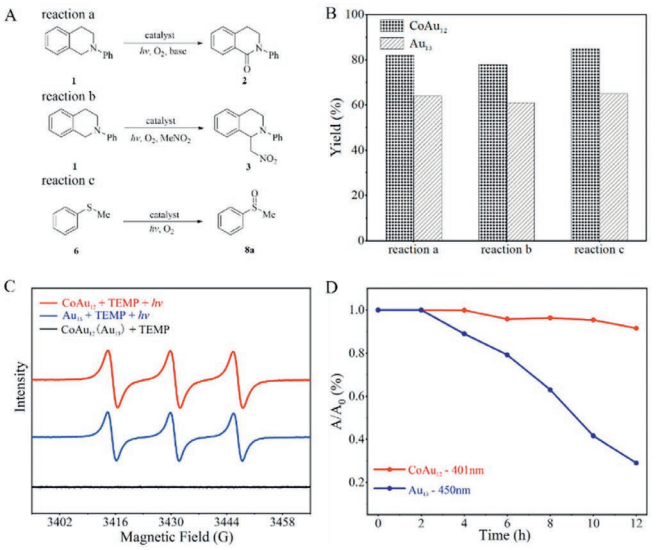


Fig. 3. (A) Three model reactions involving singlet oxygen oxidation process. (B) Yield of $CoAu_{12}$ and Au_{13} catalyzed model reactions. (C) *In-situ* EPR spectra for the detection of singlet oxygen (*hv*: blue LED irradiation). (D) The changes of characteristic UV–vis peaks of $CoAu_{12}$ at 401 nm and Au_{13} at 450 nm during catalysis.

The catalytic performance of $CoAu_{12}$ and Au_{13} in photo-induced oxidations of tetrahydroisoquinoline and sulfide were compared. Three model reactions (Fig. 3A, reactions a-c) involving singlet oxygen oxidation process were selected, and the catalytic results were shown in Fig. 3B. Both $CoAu_{12}$ and Au_{13} were catalytically active to the reactions. Interestingly, we found that $CoAu_{12}$ showed higher efficiency than Au_{13}, leading to the oxidized products in higher yields (Fig. 3B). To gain deeper insight into the catalytic mechanism of $CoAu_{12}$ and Au_{13}, we conducted *in-situ* EPR experiments. The generated singlet oxygen by $CoAu_{12}$ or Au_{13} were captured by 2,2,6,6-tetramethylpiperidine (TEMP) and detected by EPR (Fig. 3C). Additionally, 1,3-diphenylisobenzofuran (DPBF) was employed as the probe and the catalytic process of $CoAu_{12}$ and Au_{13} in O_2 activation was monitored (Fig. S8 in Supporting information). DPBF can react with single oxygen and result in the notable absorption change [52]. As shown in Fig. S8, the characteristic absorption peak of DPBF at 413 nm decreased under light irradiation when it was mixed with $CoAu_{12}$ or Au_{13} in the presence of O_2, while its absorption spectrum kept basically unchanged under the conditions without nanoclusters. The above experimental results demonstrate that both $CoAu_{12}$ and Au_{13} are capable of activating O_2 under irradiation, producing singlet oxygen. What is the reason for their different catalytic activities? Time-dependent UV–vis spectra of $CoAu_{12}$ and Au_{13} under the reaction conditions revealed the origin of their catalytic difference (Fig. 3D). Both $CoAu_{12}$ and Au_{13} kept their structures at the early stage of the catalytic process based on their unchanged absorptions in the first 2 h. However, it was found that the characteristic absorption peak of Au_{13} at 450 nm disappeared rapidly accompanied by the progress of the catalytic reaction. In sharp contrast, the characteristic absorption peak of $CoAu_{12}$ at 401 nm kept basically unchanged during the reaction. This result indicates that the different catalytic activities of $CoAu_{12}$ and Au_{13} are mainly attributed to their different structural durability during catalysis. The robust structure and high O_2 activation efficiency of $CoAu_{12}$ under light irradiation and atmospheric

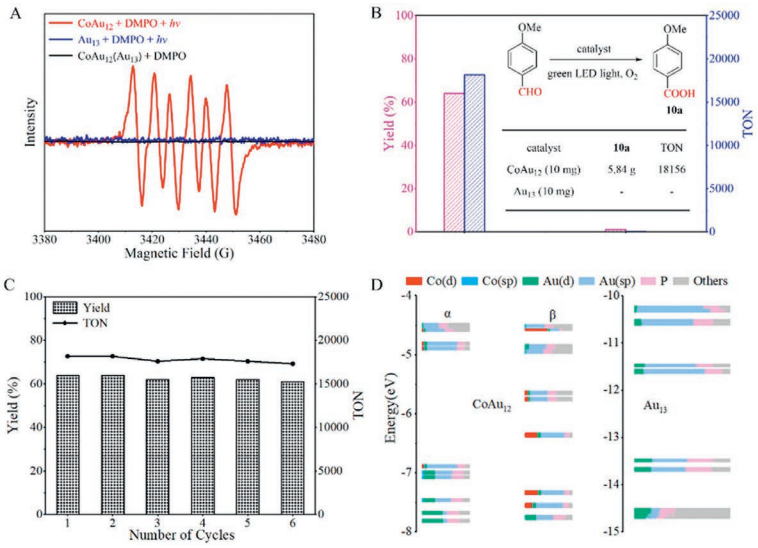


Fig. 4. (A) EPR experiments for the detection of superoxide (*hv*: green LED irradiation). (B) Yields and TONs of $CoAu_{12}$ and Au_{13} catalyzed oxidation of aldehyde **6** for the formation of carboxylic acid **7**. (C) Recycling experiments of $CoAu_{12}$ catalyzed large-scale reaction from **6** to **7**. (D) Calculated energies of molecular orbitals of $CoAu_{12}$ and Au_{13}.

oxygen contributes to its exceptional catalytic performance in oxidation reactions.

Apart from high stability, $CoAu_{12}$ showed unique catalytic activity that Au_{13} does not have. We found that $CoAu_{12}$ not only facilitated the generation of singlet oxygen, but also activated O_2 and produced superoxide under light irradiation. The free radical scavenger 5,5-dimethyl-1-pyrroline-*N*-oxide (DMPO) was used to identify superoxide. Control experiments were conducted and the typical signals of [DMPO–$O_2^{\bullet-}$] combined with the oxidized DMPO [DMPO–$O^{\bullet}$] [53] were observed when $CoAu_{12}$ was used under blue LED irradiation, verifying the catalytic ability of $CoAu_{12}$ in converting O_2 to superoxide. In contrast, Au_{13} gave negligible signals. This comparison is particularly significant under green LED irradiation. Obvious and exclusive of the superoxide occurred when $CoAu_{12}$ was employed while none of signal was observed with Au_{13} (Fig. 4A). This result, combined with the above investigation of nanocluster catalysis in the model oxidation reactions, unambiguously indicate that the excited $CoAu_{12}$ under light irradiation is able to activate O_2 by energy transfer as well as electron transfer, thus producing both singlet oxygen and superoxide. In sharp contrast, the excited Au_{13} can only undergo energy transfer with O_2 and trigger the generation of singlet oxygen. The dual activation pathways of $CoAu_{12}$ would enable its efficient catalysis in oxidation of aldehydes based on the previous reports [54]. The catalytic oxidation of aldehyde for the formation of carboxylic acid was selected for evaluating the catalytic performance of $CoAu_{12}$. $CoAu_{12}$ catalyzed the oxidation of aldehydes efficiently, giving **10a** in 84 % yield, while Au_{13} showed negligible catalytic activity under the same reaction conditions (details in Supporting information). Concerning the structural robustness as well as the high catalytic efficiency of $CoAu_{12}$ nanocluster, a large-scale reaction was then carried out to manifest the practicality of $CoAu_{12}$ catalysis (Fig. 4B and Fig. S10 in Supporting information). 5.84 g of carboxylic acid **10a** were obtained in the presence of only 10.0 mg of $CoAu_{12}$ catalyst under green light irradiation. Thus, the TON of the large-scale reaction was calculated to be as high as 18,156. Owing to its structural robustness under light irradiation and oxidation conditions, $CoAu_{12}$ was able to be recovered and recycled for at least 6 times without obvious loss of catalytic activity in the large-scale experiments (Fig. 4C). The recovered $CoAu_{12}$ demonstrated the identical UV–vis and ESI-MS spectra with that of the freshly prepared one (Fig. S11 in Supporting information), indicating the structural durability of $CoAu_{12}$ nanocluster during catalysis. Substrate scope investigation further verifies the applicability of $CoAu_{12}$ catalysis in a broad spectrum of organic transformations (Figs. S16-S18 in Supporting information).

To gain deeper insight into the origin of catalytic capability of $CoAu_{12}$ in converting O_2 to superoxide, we conducted experimental as well as calculated studies. Based on the DPV (Fig. 2C) and emission spectra (Fig. S12 in Supporting information), the oxidation potential of the excited $CoAu_{12}$ was estimated to be −1.42 V [34]. This value is much lower than the reduction potential from O_2 to superoxide radical anion $O_2^{\bullet-}$ (−0.91 V) [55,56]. In other words, $CoAu_{12}$ is able to reduce O_2 and generate superoxide under light irradiation. In contrast, the oxidation potential of the excited Au_{13} was estimated to be about −0.80 V (calculated based on the DPV spectrum in Fig. 3C and emission spectra in Fig. S12), demonstrating that Au_{13} is difficult to reduce O_2 and generate superoxide under light irradiation. Apart from the photo redox studies, it should be noted that $CoAu_{12}$ has the unpaired electron, which has been confirmed by EPR spectrum (Fig. 2A) and the calculated spin density distribution (Fig. S14). Upon excitation, $CoAu_{12}$ favors to transfer the unpaired electron to O_2, leading to the generation of superoxide, while the electron transfer process between Au_{13} and O_2 is less favorable because of its closed-shell electronic structure. Calculations indicate that the energy level of the single occupied molecular orbital (SOMO) of $CoAu_{12}$ is −6.36 eV, while the energy level of the highest occupied molecular orbital (HOMO) of Au_{13} is −13.48 eV (Fig. 4D). Meanwhile, the calculated vertical ionization potential (details in Supporting information) of $CoAu_{12}$ (7.9 eV) is much lower than that of Au_{13} (14.4 eV). The theoretical results also suggest that $CoAu_{12}$ is more favorable than Au_{13} to transfer an electron to O_2 and produce the superoxide radical anion.

In summary, we synthesized the first cobalt-kernelled metal nanocluster $CoAu_{12}$ in this work. Structural analysis reveals its symmetric and contracted kernel compared to 4d and 5d metal-kernelled MAu_{12} nanocluster system. $CoAu_{12}$ possesses unique electronic structure that disobeys the octet rule. Its unpaired electron was discovered and verified based on experimental and theoretical results. $CoAu_{12}$ features both structural stability and catalytic activity under oxidation and light irradiation conditions, catalyzing oxidation reactions involving singlet oxygen. Especially, $CoAu_{12}$ demonstrates electron transfer activity with oxygen apart from the energy transfer activity. It was applied for the efficient

aldehyde oxidation reaction, which is not accessible by employing structurally similar and undoped Au_{13} nanocluster. Given that $CoAu_{12}$ demonstrates structural robustness and high catalytic efficiency with TON up to 18,000 in the light-induced oxidation reactions, this nanocluster is a promising catalyst in photocatalysis. The oxidation products of these types of light-induced catalytic reactions can serve as intermediates in organic synthesis and biopharmaceutical production, driving the application of nanoclusters in the field of photocatalysis. We expect that the work of synthesis, structure, and catalytic investigations of $CoAu_{12}$ nanocluster would stimulate more research on Co-doped gold nanoclusters and facilitate the discovery of their unique structures and properties.

Declaration of competing interest

The authors declare no competing financial interest.

CRediT authorship contribution statement

Hao Liu: Methodology, Investigation, Formal analysis, Data curation. **Kang Li:** Software, Resources, Formal analysis, Data curation. **Fengyi Li:** Formal analysis, Data curation. **Yan Zhao:** Data curation. **Weigang Fan:** Data curation. **Yong Pei:** Writing – review & editing, Methodology, Investigation, Funding acquisition, Formal analysis, Data curation. **Man-Bo Li:** Writing – review & editing, Writing – original draft, Validation, Supervision, Project administration, Methodology, Funding acquisition, Formal analysis, Data curation, Conceptualization.

Acknowledgments

This work was supported by the National Natural Science Foundation of China (Nos. 22422101, 22371002, 92061110, 22373082, 91961121), the Innovation and Entrepreneurship Project of Overseas Returnees in Anhui Province (No. 2022LCX014), the Science and Technology Innovation Program of Hunan Province (No. 2023RC1055), and the Project of Innovation Team of the Ministry of Education (No. IRT_17R90). We thank the staff members of the Electron Spin Resonance System (https://cstr.cn/31125.02.SHMFF.ESR) at the Steady High Magnetic Field Facility, CAS (https://cstr.cn/31125.02.SHMFF), for providing technical support and assistance in date collection and analysis.

Supplementary materials

Supplementary material associated with this article can be found, in the online version, at doi:10.1016/j.cclet.2025.111230.

References

[1] M. Zhu, C. Aikens, M.F.J. Hollander, et al., J. Am. Chem. Soc. 130 (2008) 5883–5885.
[2] Q. Yao, L. Liu, S. Malola, et al., Nat. Chem. 15 (2023) 230–239.
[3] Z. Lei, J.J. Li, Z. A, et al., Angew. Chem. Int. Ed. 60 (2021) 14415–14419.
[4] Y. Shichibu, Y. Negishi, T. Watanabe, et al., J. Phys. Chem. C 111 (2007) 7845–7847.
[5] J.S. Yang, Y.J. Zhao, X.M. Li, et al., Angew. Chem. Int. Ed. 63 (2024) e202318030.
[6] Y. Li, Y. Song, X. Zhang, et al., J. Am. Chem. Soc. 144 (2022) 12381–12389.
[7] Y.H. Xu, W.J. Tian, A. Muñoz-Castro, et al., Science 382 (2023) 840–843.
[8] K. Xiao, Y. Xue, B. Yang, et al., CCS Chem. 3 (2021) 555–565.
[9] J.J. Zhang, Y. Wu, Y. Li, et al., Chin. Chem. Lett. 36 (2025) 111003.
[10] C.P. Joshi, M.S. Bootharaju, M.J. Alhilaly, et al., J. Am. Chem. Soc. 137 (2015) 11578–11581.
[11] W.D. Tian, W.D. Si, S. Havenridge, et al., Sci. Bull. 69 (2024) 40–48.
[12] H. Wu, G.N. Andrew, R. Anumula, et al., Chin. Chem. Lett. 35 (2024) 108340.
[13] T.A.D. Nguyen, Z.R. Jones, B.R. Goldsmith, et al., J. Am. Chem. Soc. 137 (2015) 13319–13324.
[14] W.D. Si, C. Zhang, M. Zhou, et al., Sci. Adv. 9 (2023) eadg3587.
[15] T. Jia, Z.J. Guan, C. Zhang, et al., J. Am. Chem. Soc. 145 (2023) 10355–10363.
[16] Q. Li, F.Y. Fu, M.Y. Zhao, et al., Chin. Chem. Lett. 36 (2025) 110090.
[17] W.D. Si, C. Zhang, M. Zhou, et al., Sci. Adv. 10 (2024) eadm6928.
[18] J.S. Yang, Y.J. Zhao, X.M. Li, et al., Angew. Chem. Int. Ed. 63 (2024) e202318030.
[19] W.D. Si, Y.Z. Li, S.S. Zhang, et al., ACS Nano 15 (2021) 16019–16029.
[20] J. Yan, H. Su, H. Yang, S. Malola, et al., J. Am. Chem. Soc. 137 (2015) 11880–11883.
[21] X. Du, P. Pan, H. Li, et al., Chin. Chem. Lett. 36 (2025) 111155.
[22] Y. Shichibu, K. Konishi, Small 6 (2010) 1216–1220.
[23] J.B. Patty, S. Havenridge, D. Tietje-Mckinney, et al., J. Am. Chem. Soc. 144 (2022) 478–484.
[24] M.R. Narouz, S. Takano, P.A. Lummis, et al., J. Am. Chem. Soc. 41 (2019) 14997–15002.
[25] P. Luo, X.J. Zhai, S. Bai, Y.B. Si, et al., Angew. Chem. Int. Ed. 62 (2023) e202219017.
[26] C. Yao, Y.J. Lin, J. Yuan, et al., J. Am. Chem. Soc. 137 (2015) 15350–15353.
[27] L. Liao, S. Zhou, Y. Dai, et al., J. Am. Chem. Soc. 137 (2015) 9511–9514.
[28] W. Fei, S. Antonello, T. Dainese, et al., J. Am. Chem. Soc. 141 (2019) 16033–16045.
[29] Z. Qin, S. Sharma, C.Q. Wan, et al., Angew. Chem. Int. Ed. 60 (2021) 970–975.
[30] K. Kwak, Q. Tang, M. Kim, et al., J. Am. Chem. Soc. 137 (2015) 10833–10840.
[31] E. Ito, S. Takano, T. Nakamura, et al., Angew. Chem. Int. Ed. 60 (2021) 645–649.
[32] X. Liu, G. Saranya, X. Huang, et al., Angew. Chem. Int. Ed. 59 (2020) 13941–13946.
[33] S. Hossain, Y. Niihori, L.V. Nair, et al., Acc. Chem. Res. 51 (2018) 3114–3124.
[34] Y. Zhang, S.R. He, Y. Yang, et al., J. Am. Chem. Soc. 145 (2023) 12164–12172.
[35] Y. Zhang, W. Zhang, T.S. Zhang, et al., J. Am. Chem. Soc. 146 (2024) 9631–9639.
[36] J.Q. Fan, Y. Yang, C.B. Tao, et al., Angew. Chem. Int. Ed. 63 (2023) e202215741.
[37] J.Q. Fan, Y. Li, W.W. Xu, et al., Angew. Chem. Int. Ed. 63 (2024) e202413861.
[38] T.S. Zhang, W. Fei, N. Li, et al., Nano Lett. 23 (2023) 235–242.
[39] C. Liu, Y. Zhao, T.S. Zhang, et al., Nat. Commun. 14 (2023) 3730.
[40] Y. Zhao, Z.M. Zhu, W. Fan, et al., Nat. Commun. 15 (2024) 9632.
[41] S. Takano, S. Ito, T. Tsukuda, J. Am. Chem. Soc. 141 (2019) 15994–16002.
[42] H. Hirai, S. Takano, T. Nakamura, et al., Inorg. Chem. 59 (2020) 17889–17895.
[43] H. Hirai, S. Takano, T. Nakashima, et al., Angew. Chem. Int. Ed. 61 (2022) e202207290.
[44] Y. Fukumoto, T. Omoda, H. Hirai, et al., Angew. Chem. Int. Ed. 63 (2024) e202402025.
[45] J. Zhang, Y. Zhou, K. Zheng, et al., Nano Res. 11 (2018) 5787–5798.
[46] K. Kwak, Q. Tang, M. Kim, et al., J. Am. Chem. Soc. 137 (2015) 10833–10840.
[47] S.S. Zhang, L. Feng, R.D. Senanayake, et al., Chem. Sci. 9 (2018) 1251–1258.
[48] S. Jin, W. Du, S. Wang, et al., Inorg. Chem. 56 (2017) 11151–11159.
[49] W.W. Xu, X.C. Zeng, Y. Gao, Acc. Chem. Res. 51 (2018) 2739–2747.
[50] M. Walter, J. Akola, O. Lopez-Acevedo, et al., Proc. Nat. Acad. Sci. U. S. A. 105 (2008) 9157–9162.
[51] S. Wang, L. Tang, B. Cai, et al., J. Am. Chem. Soc. 144 (2022) 3787–3792.
[52] Y. Zhou, W. Gu, R. Wang, et al., Nano Lett. 24 (2024) 2226–2233.
[53] L. Chen, J. Duan, P. Du, et al., Water Res. 221 (2022) 118747.
[54] J.P. Yuan, Z.J. Guan, H.Y. Lin, et al., Angew. Chem. Int. Ed. 62 (2023) e202303896.
[55] M. Hayyan, M.A. Hashim, I.M. AlNashef, Chem. Rev. 116 (2016) 3029–3085.
[56] R.G. Evans, O.V. Klymenko, S.A. Saddoughi, et al., J. Phys. Chem. B 108 (2004) 7878–7886.